batteries

MDPI

Review

Redox Evolution of Li-Rich Layered Cathode Materials

Liang Fang [1], Mingzhe Chen [2,*], Kyung-Wan Nam [1,*] and Yong-Mook Kang [3,4,*]

[1] Department of Energy and Materials Engineering, Dongguk University-Seoul, Seoul 04620, Korea
[2] School of Energy and Power Engineering, Nanjing University of Science and Technology, Nanjing 210094, China
[3] Department of Materials Science and Engineering, Korea University, Seoul 04620, Korea
[4] KU-KIST Graduate School of Converging Science and Technology, Korea University, Seoul 02841, Korea
* Correspondence: chenmingzhe@njust.edu.cn (M.C.); knam@dongguk.edu (K.-W.N.); dake1234@korea.ac.kr (Y.-M.K.)

Abstract: Li-rich layered oxides utilizing reversible oxygen redox are promising cathodes for high-energy-density lithium-ion batteries. However, they exhibit different electrochemical profiles before and after oxygen redox activation. Therefore, advanced characterization techniques have been developed to explore the fundamental understanding underlying their unusual phenomenon, such as the redox evolution of these materials. In this review, we present the general redox evolution of Li-rich layered cathodes upon activation of reversible oxygen redox. Various synchrotron X-ray spectroscopy methods which can identify charge compensation by cations and anions are summarized. The case-by-case redox evolution processes of Li-rich 3d/4d/5d transition metal O3 type layered cathodes are discussed. We highlight that not only the type of transition metals but also the composition of transition metals strongly affects redox behavior. We propose further studies on the fundamental understanding of cationic and anionic redox mixing and the effect of transition metals on redox behavior to excite the full energy potential of Li-rich layered cathodes.

Keywords: lithium-ion battery; Li-rich layered cathodes; synchrotron characterization techniques; redox evolution; mixed cationic and anionic redox

check for updates

Citation: Fang, L.; Chen, M.; Nam, K.-W.; Kang, Y.-M. Redox Evolution of Li-Rich Layered Cathode Materials. *Batteries* **2022**, *8*, 132. https://doi.org/10.3390/batteries8100132

Academic Editor: Carlos Ziebert

Received: 19 August 2022
Accepted: 16 September 2022
Published: 21 September 2022

1. Introduction

Lithium-ion batteries (LIBs), as energy storage devices, play a vital role in daily life [1,2]. The salient goal of future LIBs development is to increase the energy density while reducing the price [3–7]. For a long time, cathode materials have been critically limiting the energy densities of LIBs [8–10], because the conventional cathode materials depending on cationic redox can only provide capacities lower than 200 mAh g^{-1} [11,12]. Meanwhile, Li-rich layered oxide cathodes utilizing reversible oxygen redox as well as cationic redox can provide capacities higher than 260 mAh g^{-1}, making them attractive as potential candidates for future LIBs with higher energy densities [13–17]. Distinct from conventional cathode materials, Li-rich layered cathodes always exhibit different charge-discharge curves after oxygen redox activation [18,19]. Hence, a lot of efforts have been dedicated to uncovering the redox evolution behind this phenomenon [20–24].

With the development of synchrotron characterization techniques, cationic and anionic redox in Li-rich layered cathodes can be somewhat clearly identified [25–27]. The charge compensation mechanism based on cationic redox has been well characterized by hard X-ray absorption spectroscopy (XAS) since 2011 [20,28]. Oxygen redox behavior of Li-rich layered cathodes has been disclosed by soft XAS and Resonant inelastic X-ray scattering (RIXS) in 2016 and hard X-ray photoelectron spectroscopy (HAXPES) in 2017 [19,21]. Mapping RIXS (mRIXS) was developed to provide a fingerprint signal of oxygen redox in 2018 [29]. High-resolution RIXS (HR-RIXS) verified O_2 as the oxidation state of O^{2-} in the oxygen redox in 2020 [24].

Thanks to these successive endeavors to identify cationic and anionic redox, the redox evolution of Li-rich layered cathodes could be understood and described more or less. Although the redox behaviors of different Li-rich layered cathodes have been investigated by various techniques and listed in separate research papers, a universal summary and outlook of the redox evolution of Li-rich layered cathodes, particularly employing the state-of-the-art synchrotron characterizations, are still lacking. In this review, the general redox evolution of Li-rich layered cathodes is summarized and compared with the redox behavior of conventional cathodes. Synchrotron characterization techniques employed to study charge compensation mechanisms of cationic and anionic redox are then discussed. Finally, the case-by-case studies of the redox evolution of Li-rich 3d/4d/5d transition metal layered cathodes are presented and discussed one after another. This work highlights that not only the type of transition metals but also the composition of transition metals strongly affects the redox behavior of Li-rich layered cathodes. Future studies should investigate why cationic and anionic redox rearranges and coincides after oxygen redox activation and how transition metals affect redox behavior. Such insights will guide us to reach the full potential of Li-rich layered cathodes toward higher energy densities for future LIBs.

2. Types of Redox Behavior

The cathode materials undergo lithium-ion intercalation and deintercalation processes in rechargeable LIBs [30]. Classical cathode materials, such as $LiMn_2O_4$ [31], $LiFePO_4$ [32], $LiCoO_2$ [33], and $LiNi_xCo_yMn_{1-x-y}O_2$ [34–36], involve cationic redox of transition-metal ions. The schematic diagram of their redox behavior is shown in Figure 1a. During charge/discharge, lithium ions are extracted/inserted from/into the structure, while electrons are withdrawn/inserted from/into cations. Since their host structure is maintained, the charge-discharge curves are stable and symmetrical. Typical Li-rich layered cathodes with reversible anionic redox exhibit a distinct redox behavior, as shown in Figure 1b. The representative Li-rich layered cathodes are $Li_{1.2}Ni_{0.2}Mn_{0.6}O_2$ [13], $Li_{1.2}Ni_{0.13}Co_{0.13}Mn_{0.54}O_2$ [14], $Li_2Ru_{0.75}Sn_{0.25}O_3$ [18], etc. Their first cycle charging process involves distinctive cation and anion oxidations. Since a structural rearrangement occurs during the activation of anionic redox in the first cycle charging process as evidenced by X-ray powder diffraction and transmission electron microscopy, cation and anion reductions become merged from the first cycle discharge to the subsequent charge-discharge cycles [24]. Hence, the feature of the first cycle charge curve differs from the subsequent charge-discharge curves. Meanwhile, the subsequent charge-discharge curves exhibit relative stability and symmetry even though voltage decay and minor asymmetric redox occur.

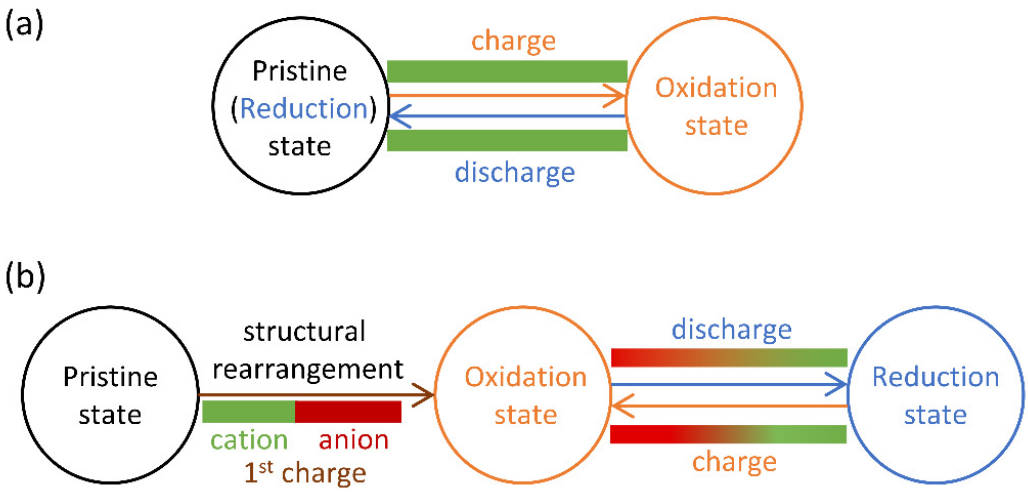

Figure 1. The schematic diagrams of redox evolution in (**a**) conventional cathodes and (**b**) Li-rich layered cathodes.

3. Characterization Techniques

Understanding the redox behavior in Li-rich layered cathodes has been constantly updated with the development of synchrotron X-ray characterization techniques. Synchrotron X-ray spectroscopy has been well suited to identify the valence states of elements in cathode materials during charge-discharge. Ex-situ, in-situ, and in-operando measurements can be selected by purpose and experimental requirements [26,37].

X-ray photoelectron spectroscopy (XPS) can determine the density of electronic states of materials, but it is surface-sensitive [38,39]. Hard X-ray photoelectron spectroscopy (HAXPES) using focused synchrotron X-ray beams with tunable energy can probe deeper information (Figure 2a) [21,40,41]. Figure 2b shows the spectra of Mn $2p_{3/2}$ orbital at two different states of discharge. The deconvolution of spectra can identify the existence and amount of Mn^{3+}. The oxygen redox in the bulk materials can be verified by the O 1s spectra with high X-ray energy (Figure 2c). Even though identifying the valence state of transition metals and oxygen is feasible by HAXPES, quantitative analysis is challenging due to the peak overlapping.

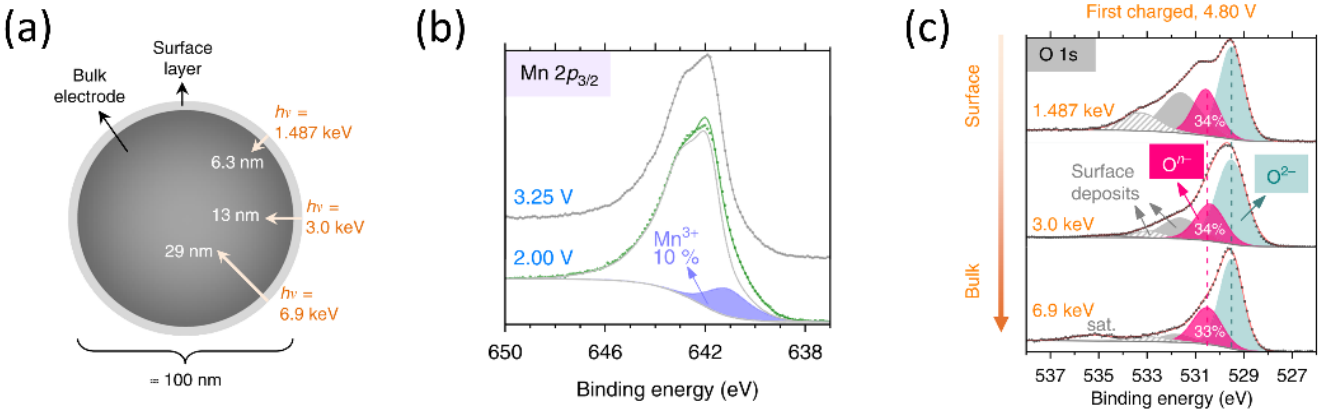

Figure 2. (**a**) The detection depth of HAXPES; The HAXPES of (**b**) Mn and (**c**) O at different charge-discharge states of $Li_{1.2}Ni_{0.13}Mn_{0.54}Co_{0.13}O_2$. Reproduced with permission from Ref. [21] Copyright 2017, Nature Portfolio.

X-ray absorption near edge structure (XANES) and extended X-ray absorption fine structure (EXAFS) have been widely used to determine the electronic and local structure and coordination environment in an elemental selective manner [19,20,22,23,42–46]. Figure 3a shows the schematic diagram of hard XAS in transmission mode. Compared with XPS, which only probes the surface less than a few nm, hard XAS provides bulk information. Therefore, hard XAS has been widely applied to determine the oxidation state and geometry of 3d/4d transition metals. Typical K-edge XAS spectra explored for Li-rich layered cathodes include Ni, Co, Mn, and Ru. Figure 3b shows the in-situ XANES spectra of Ni, Co, and Mn during the first charging process. In general, the whole spectra shift to higher energy indicates the oxidation of transition metals, such as the spectra of Ni and Co. Meanwhile, the local structural rearrangement of transition metals influences the shape of spectra even though the oxidation state remains the same, such as the Mn spectra. EXAFS results can also reveal the oxidation state of transition metals, as the shorter transition metals to oxygen distances the higher oxidation states. For example, the decrease in Co-O and Ni-O distances in Figure 3c indicate the oxidation of Co and Ni, which is consistent with the XANES results in Figure 3b. The Mn-O distance exhibits negligible change, indicating Mn remains 4+. Since the oxidation state changes of transition metals show distinguishable XANES spectra, quantitative analysis of the oxidation state changes is feasible by comparing the spectra of reference compounds with known oxidation states [47].

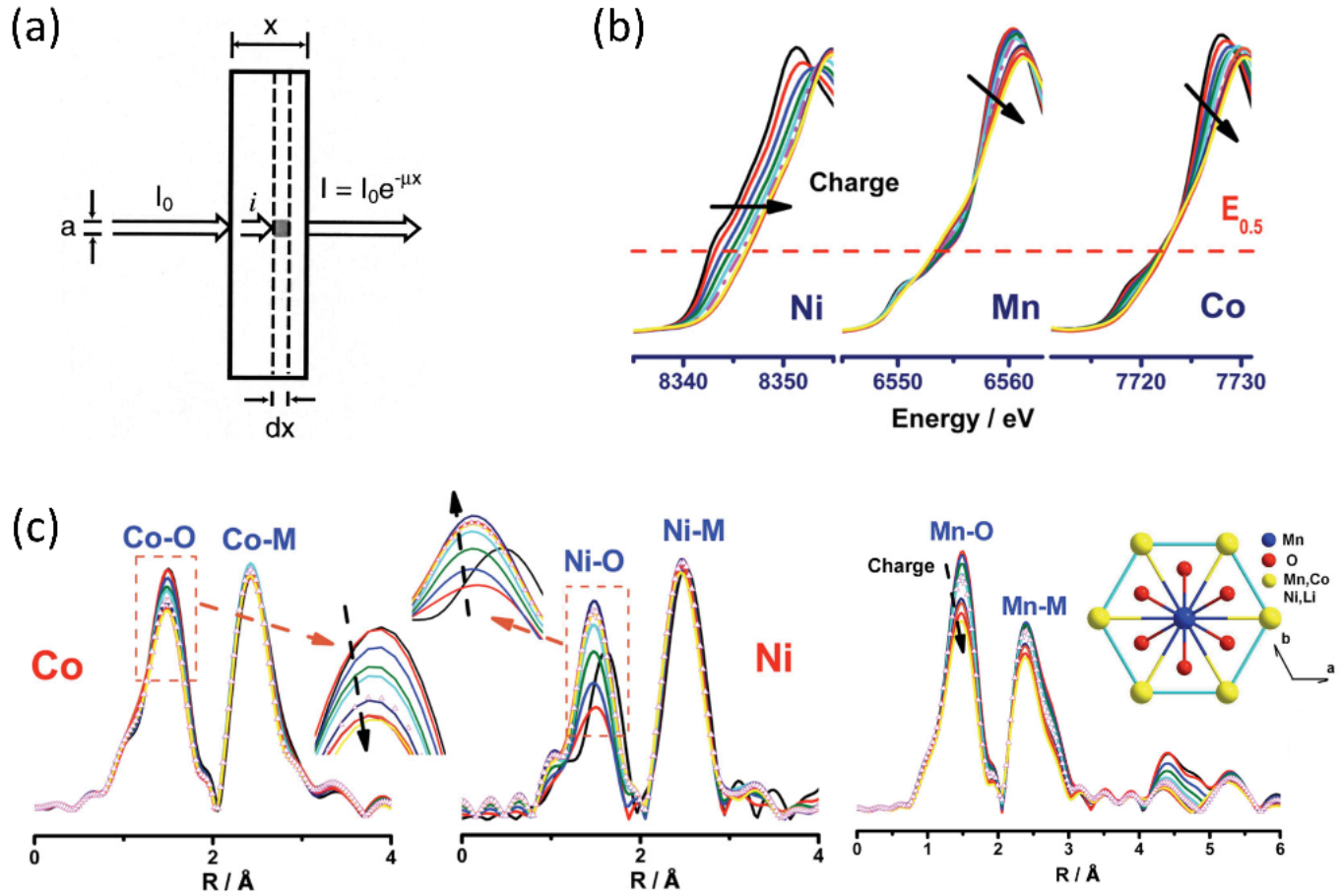

Figure 3. (**a**) The transmission detection mode of hard XAS; (**b**) In-situ XAS spectra of Ni, Co, and Mn during the first cycle charge process of $Li_{1.2}Ni_{0.15}Co_{0.1}Mn_{0.55}O_2$; (**c**) The EXAFS results of Ni, Co, and Mn in R space. Reproduced with permission from Refs. [20,42]. Copyright 2000, American Physical Society. Copyright 2014, Wiley-VCH.

Soft XAS can prove not only the oxidation state of transition metals but, more importantly, the oxidation state of oxygen [19,46,48–54]. Several detections and imaging methods are developed based on soft XAS, including total electron yield (TEY) mode, total fluorescence yield (TFY) mode, fluorescence yield X-ray microscopy (FY-XRM), and scanning transmission X-ray microscopy (STXM). Their major differences lie in the detection depths (Figure 4a). Figure 4b shows the oxygen K-edge spectra detected by the above methods. STXM-XAS is a unique technique as it probes the bulk information and provides a clear oxygen oxidation signal compared to other XAS methods. Additionally, the 2D mapping capability of STXM-XAS provides chemical and oxidation state distributions over the cathode particles with nano-meter spatial resolution in an elemental selective manner. Soft XAS can also identify the oxidation state of transition metals, as different oxidation states of transition metals depict distinct spectra shapes. For example, the soft XAS spectra of Mn^{3+} and Mn^{4+} L-edge are distinguishable, as shown in Figure 4c.

Recently, RIXS has emerged as a powerful tool for identifying oxygen redox [24,29,53,55–63]. It can scan both incident and emitted X-rays, so electrons occupying different energy states can be distinguished (Figure 5a). Furthermore, mRIXS established at Advanced Light Source at Lawrence Berkeley National Laboratory has become persuasive evidence for oxygen redox as the oxygen redox signal can be clearly separated from other signals (Figure 5b). HR-RIXS developed at Diamond Light Source's I21 beamline provides further evidence that O_2 molecules are formed as oxidized species of O^{2-} (Figure 5c,d).

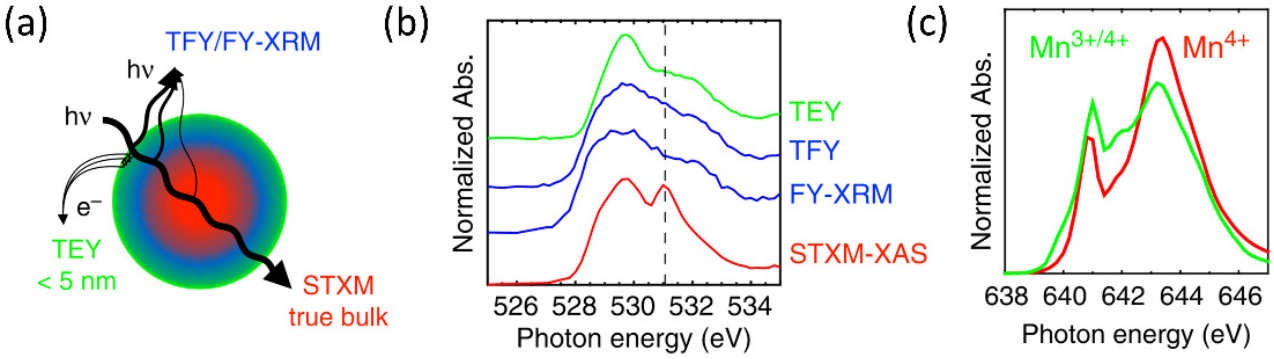

Figure 4. (**a**) Schematic comparing of XAS in various modes; (**b**) The oxygen K-edge XAS spectra collected in various modes; (**c**) The Mn L-edge XAS spectra detected by STXM. The chemical composition is $Li_{1.17}Ni_{0.21}Co_{0.08}Mn_{0.54}O_2$. Reproduced with permission from Ref. [51] Copyright 2017, Nature Portfolio.

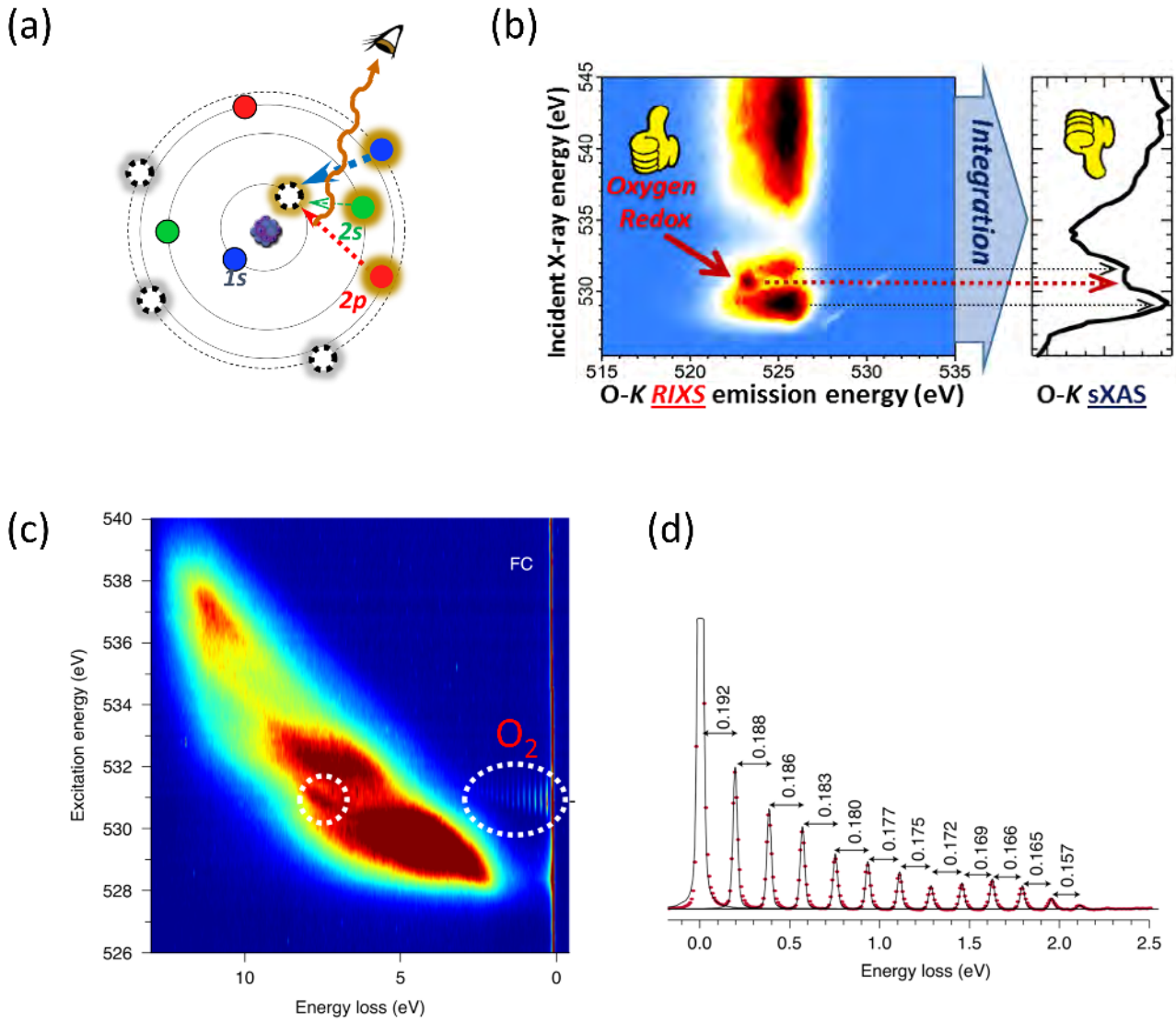

Figure 5. (**a**) Schematic of RIXS; (**b**) mRIXS map of O K-edge compared with corresponding XAS spectrum of $Li_{1.2}Ni_{0.2}Mn_{0.6}O_2$. (**c**) HR-RIXS map of O K-edge and (**d**) the low-energy loss feature of $Li_{1.2}Ni_{0.13}Co_{0.13}Mn_{0.54}O_2$. Reproduced with permission from Refs. [24,29] Copyright 2018, Elsevier. Copyright 2020, Nature Portfolio.

4. Redox Evolution of Li-Rich Layered Cathode Materials

Thanks to the development of X-ray spectroscopy, the redox evolution of Li-rich 3d/4d transition metal layered cathodes during charge-discharge is well characterized. The redox behavior of O3-type Li-rich layered cathodes with varying transition metals is discussed individually.

The structure of Li_2MnO_3 (i.e., $Li(Li_{1/3}Mn_{2/3})O_2$) is shown in Figure 6a [64], where 1/3 of Mn^{4+} is replaced by the ordered lithium in the transition metal layer. The first cycle charge-discharge curves and the charge compensation mechanism are shown in Figure 6b [61]. It is well-known that the Mn3+/4+ redox is activated after the first charge, as proved by previous XANES studies [65]. However, it has only recently been confirmed by mRIXS and soft XAS that the redox of Mn^{4+}/Mn^{7+} and oxygen is not involved during cycling [53,61]. This is because Mn^{4+} cannot be oxidized to Mn^{7+}, and oxygen gas is generated during the first charging process, followed by oxygen release from the particle surface. Therefore, only the Mn^{2+}/Mn^{4+} redox is retained, while the reversible oxygen redox is unstable in the pure Li_2MnO_3 phase.

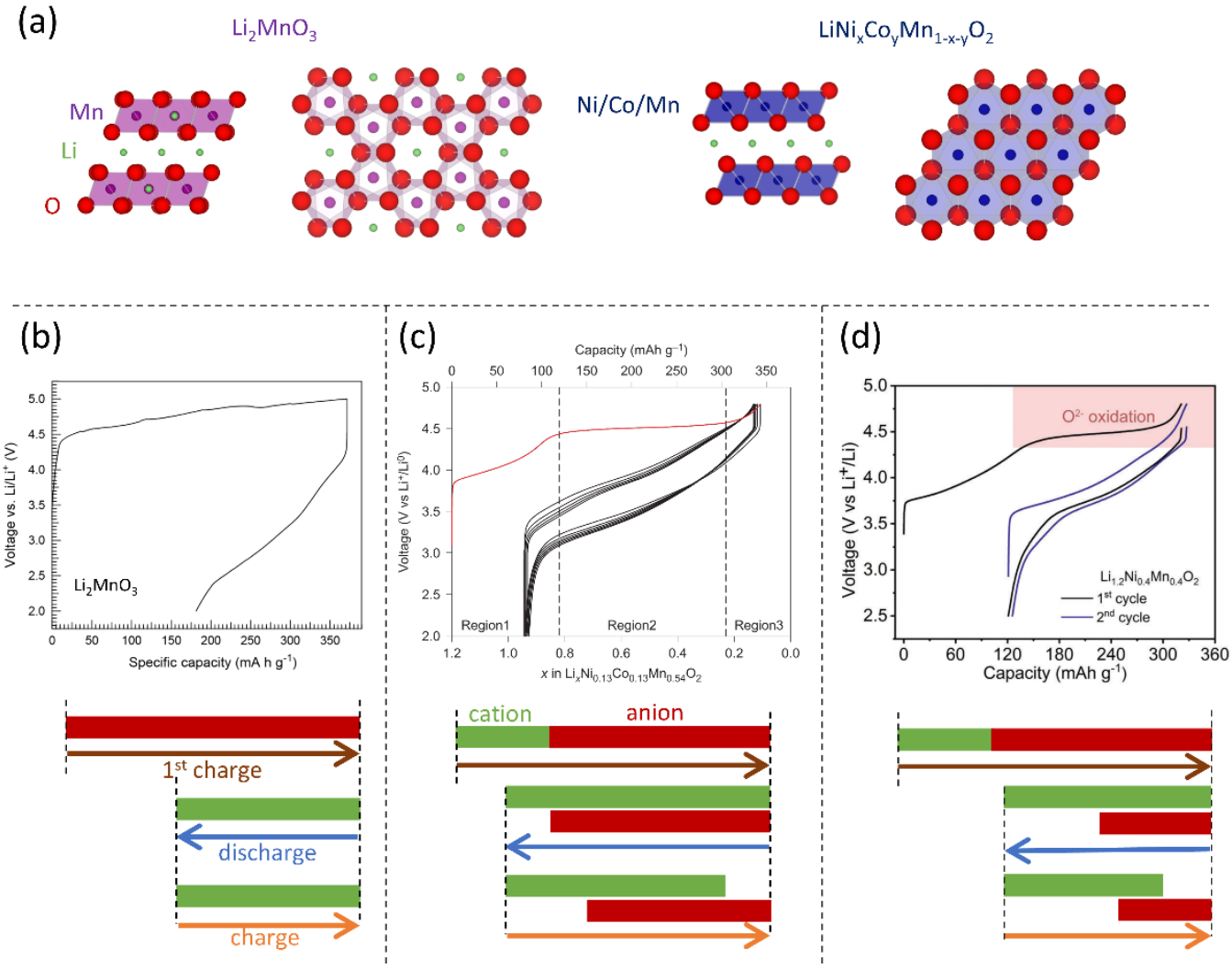

Figure 6. (**a**) The crystal structures of Li_2MnO_3 and $LiNi_xCo_yMn_{1-x-y}O_2$. The charge-discharge curves and redox evolution of (**b**) Li_2MnO_3, (**c**) $Li_{1.2}Ni_{0.13}Co_{0.13}Mn_{0.54}O_2$, and (**d**) $Li_{1.2}Ni_{0.4}Mn_{0.4}O_2$. Reproduced with permission from [19,54,61]. Copyright 2020, American Chemical Society. Copyright 2016, Nature Portfolio. Copyright 2022, Wiley-VCH.

Two phases co-exist to form a typical Li-rich 3d transition metal layered cathode, Li_2MnO_3 and $LiNi_xCo_yMn_{1-x-y}O_2$ phase (Figure 6a) [14]. The representative one with reversible oxygen redox is $Li_{1.2}Ni_{0.13}Co_{0.13}Mn_{0.54}O_2$ ($0.5Li_2MnO_3 \bullet 0.5LiNi_{1/3}Co_{1/3}Mn_{1/3}O_2$) [19]. Its charge-discharge curves and redox evolution are shown in Figure 6c, which are summarized from reported XANES and HR-RIXS results [19,24,45]. During the first charging, the cations are first oxidated to 4+ below 4.3 V, then O^{2-} is oxidated to O_2 gas around 4.5 V, where the oxidation process of cations and anions is well separated. During the first discharging process, the cations and anions are reduced simultaneously. Notably, cations and anions are oxidized during the second cycle charging process as in the first discharging process. The distinct feature is that most cations are oxidized below 4.3 V, while anions are oxidized at high voltage (>3.7 V). Distinctive from the first charging curve, the charge-discharge curves retain their feature during the following cycles, suggesting that the first discharging and the second charging process represent the redox behavior.

The composition of Li-rich 3d transition metal layered cathodes can alter the shape of charge-discharge curves and corresponding redox behavior, as shown in Figure 6d for the $Li_{1.2}Ni_{0.4}Mn_{0.4}O_2$ case [54]. The first charging process is similar to $Li_{1.2}Ni_{0.13}Co_{0.13}Mn_{0.54}O_2$, except for the smaller degree of the activation process for oxygen redox. The first discharging process also shows cationic and anionic reduction. In general, simultaneous cationic and anionic redox is observed after the first charging activation in typical Li-rich 3d transition metal layered cathodes with reversible oxygen redox.

Li-rich 4d/5d transition metal layered cathodes are also investigated to better understand the origin of anionic redox. Their structures are shown in Figure 7a. The oxidation states of Ru, Ir, and Sn in the pristine materials are 4+. The first cycle charge-discharge curves and the charge compensation mechanism of Li_2RuO_3 studied employing the in-situ XANES and HR-RIXS are shown in Figure 7b [62,66,67]. The cationic redox of Ru^{4+}/Ru^{5+} and anionic redox correspond to the well-separated stepwise voltage plateaus during the first cycle charging process. During discharge and subsequent charge processes, the cationic and anionic redox simultaneously occurs, as verified by the in-situ XANES spectra of Ru. Different from other Li-rich layered cathodes, the first cycle charge-discharge curves of Li_2IrO_3 are highly reversible (Figure 7c) [68,69]. Extensive and systematic characterization using in-situ XANES and HR-RIXS has verified that the charge compensation is exclusively associated with cationic redox rather than oxygen redox [55,62]. The voltage plateau around 3.5 V and 4.2 V corresponds to the redox of Ir^{4+}/Ir^{5+} and $Ir^{5+}/Ir^{5.5+}$, respectively.

Notably, a representative Li-rich 4d/5d transition metal layered cathode, $Li_2Ru_{0.75}Sn_{0.25}O_3$ [18], shows highly reversible oxygen redox and stable cycling performance with a similar charge compensation mechanism as in $Li_{1.2}Ni_{0.4}Mn_{0.4}O_2$ (Figure 7d). The in-situ XANES and RIXS results confirm that the first cycle oxidation plateau around 3.5 V and 4.2 V corresponds to the oxidation of Ru^{4+} and O^{2-}, respectively [18,55,62]. Moreover, the in-situ XANES spectra of Ru during the second cycle quantitatively decouple the contribution of cationic and anionic redox to the charge-discharge process [22]. After the first charging process, simultaneous cationic and anionic redox without having a clear-cut voltage is also observed in $Li_{1.2}Ni_{0.4}Mn_{0.4}O_2$.

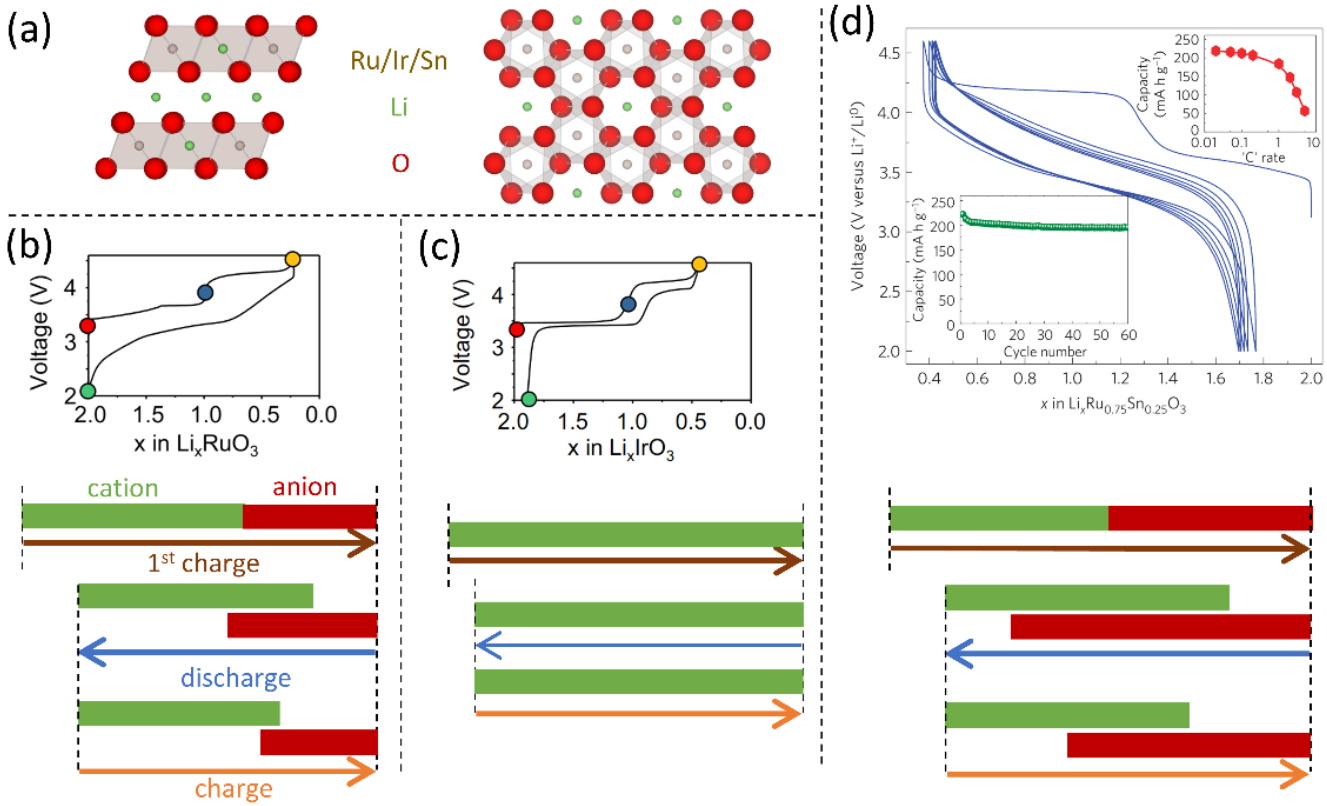

Figure 7. (**a**) The crystal structures of Li_2RuO_3, Li_2IrO_3, and Li_2SnO_3. The charge-discharge curves and redox evolution of (**b**) Li_2RuO_3, (**c**) Li_2IrO_3, and (**d**) $Li_2Ru_{0.75}Sn_{0.25}O_3$. Reproduced with permission from Refs. [18,62] Copyright 2021, Nature Portfolio. Copyright 2013, Nature Portfolio.

5. Summary and Perspectives

A universal redox evolution of Li-rich layered cathodes can be summarized as follows. During the first charging process, cationic oxidation occurs, followed by well-separated anionic oxidation, depending on the electron energy states for cation and anion redox in the pristine materials. In practice, the oxidation of Ni^{2+}/Ni^{4+}, Co^{3+}/Co^{4+}, Ru^{4+}/Ru^{5+}, and $Ir^{4+}/Ir^{5+}/Ir^{6+}$ occurs before the oxidation of O^{2-}. When the oxygen redox is not activated, the first cycle discharge curve exhibits the same shape as the charge curve with less than 0.2 V overpotential. However, when the oxygen redox is activated, the first cycle discharge curve shows a typical S-shaped with a huge voltage hysteresis compared to the first cycle charge curve. The subsequential charge-discharge curves remain S-shaped. The redox of cations and anions overlap during the S-shaped charge-discharge process. The degree of overlap during discharging is higher than that during charging.

Even though the mixture of cationic and anionic redox has been observed, the fundamental understanding of this phenomenon has been overlooked and remains unknown. The quantitive analysis of cationic and anionic redox contribution to the charge-discharge process should be investigated to understand how cationic and anionic redox mix. Li-rich layered cathodes have undesirable electrochemical properties, such as voltage decay and hysteresis. The relationship between these undesirable properties and the mixture of cationic/anionic redox should be investigated. Structural changes, such as transition metal migration, have been observed during the activation of oxygen redox in Li-rich layered cathodes. The relationship between structural changes and the cationic/anionic redox mixing should be clarified.

Transition metals strongly affect the activation and stability of oxygen redox in Li-rich layered cathodes. Li_2MnO_3, Li_2RuO_3, Li_2SnO_3, and Li_2IrO_3 show similar structures, which contain honeycomb-ordered transition metals. O^{2-} can be oxidated to O_2 in Li_2MnO_3 and Li_2RuO_3, but not in Li_2SnO_3 and Li_2IrO_3. O_2 is unstable in Li_2MnO_3 but stable in Li_2RuO_3.

Mixing multiple transition metals can stabilize and/or activate oxygen redox in Li-rich layered cathodes. The oxygen redox in the Li_2MnO_3 phase can be stabilized by the surrounding $LiMO_2$ (M indicating transition metals) phase, such as $Li_{1.2}Ni_{0.13}Co_{0.13}Mn_{0.54}O_2$. Although oxygen redox is inert in Li_2SnO_3, the mixture of Li_2SnO_3 with Li_2RuO_3 provides more reversible oxygen redox than pure Li_2RuO_3. In addition, the mixture of Li_2SnO_3 and Li_2IrO_3 can activate a huge amount of oxygen redox, but a single of them is oxygen redox inert.

Transition metals have a complicated influence on the redox behavior in Li-rich layered cathodes, which the simple electronic energy of transition metals cannot explain. The mixture of transition metals has shown positive effects on activating and stabilizing oxygen redox, the reason behind this phenomenon is a mystery. To reveal the mechanism behind the various electrochemical performances, the effect of transition metals on structural changes should be investigated.

In summary, through recent years' research of redox behavior with advanced synchrotron techniques, the general redox behavior could be clearly identified. The Li-rich layered cathodes face the structural rearrangement after activating oxygen redox and the cationic and anionic redox are mixed during the subsequential discharge and charge process. The future direction would be to understand what controls the activation amount of oxygen redox and how the mixture of cationic and anionic redox influence the electrochemical performance. The answer to these questions will be important for pushing the Li-rich layered cathodes to the maximum energy density and efficiency.

Author Contributions: Conceptualization, L.F.; writing—original draft preparation, L.F.; writing—review and editing, L.F., M.C., K.-W.N. and Y.-M.K.; supervision, M.C., K.-W.N. and Y.-M.K.; funding acquisition, M.C., K.-W.N. and Y.-M.K. All authors have read and agreed to the published version of the manuscript.

Funding: This research was funded by the National Research Foundation of Korea (NRF) under grant numbers NRF-2017M3D1A1039561, NRF-2017R1A5A1015365, NRF-2022R1A2B5B03001781, NRF-2020M3D1A1110527, and NRF-2022R1A2C2009459. This research was also supported by "the Fundamental Research Funds for the Central Universities", No. 30922010708, and the Natural Science Foundation of Jiangsu Province (Grants No. BK 20220966), the Natural Science Foundation of China (Grants No. 52202254).

Acknowledgments: This work was also supported by the KU-KIST School Program.

Conflicts of Interest: The authors declare no conflict of interest.

References

1. Armand, M.; Tarascon, J.M. Building Better Batteries. *Nature* **2008**, *451*, 652–657. [CrossRef] [PubMed]
2. Larcher, D.; Tarascon, J.M. Towards Greener and More Sustainable Batteries for Electrical Energy Storage. *Nat. Chem.* **2015**, *7*, 19–29. [CrossRef] [PubMed]
3. Schmuch, R.; Wagner, R.; Hörpel, G.; Placke, T.; Winter, M. Performance and Cost of Materials for Lithium-Based Rechargeable Automotive Batteries. *Nat. Energy* **2018**, *3*, 267–278. [CrossRef]
4. Jo, M.R.; Kim, Y.; Yang, J.; Jeong, M.; Song, K.; Kim, Y.-I.; Lim, J.-M.; Cho, M.; Shim, J.-H.; Kim, Y.-M.; et al. Triggered Reversible Phase Transformation between Layered and Spinel Structure in Manganese-Based Layered Compounds. *Nat. Commun.* **2019**, *10*, 3385. [CrossRef]
5. Rahil, A.; Partenie, E.; Bowkett, M.; Nazir, M.H.; Hussain, M.M. Investigating the Possibility of Using Second-Life Batteries for Grid Applications. *Battery Energy* **2022**, *1*, 20210001. [CrossRef]
6. Yang, L.; Chen, R.; Liu, Z.; Gao, Y.; Wang, X.; Wang, Z.; Chen, L. Configuration-Dependent Anionic Redox in Cathode Materials. *Battery Energy* **2022**, *1*, 20210015. [CrossRef]
7. Van der Ven, A.; See, K.A.; Pilon, L. Hysteresis in Electrochemical Systems. *Battery Energy* **2022**, *1*, 20210017. [CrossRef]
8. Tarascon, J.M.; Armand, M. Issues and Challenges Facing Rechargeable Lithium Batteries. *Nature* **2001**, *414*, 359–367. [CrossRef]
9. Lee, W.; Muhammad, S.; Sergey, C.; Lee, H.; Yoon, J.; Kang, Y.-M.; Yoon, W.-S. Advances in the Cathode Materials for Lithium Rechargeable Batteries. *Angew. Chem. Int. Ed. Engl.* **2020**, *59*, 2578–2605. [CrossRef]
10. Lee, G.-H.; Lau, V.W.-H.; Yang, W.; Kang, Y.-M. Utilizing Oxygen Redox in Layered Cathode Materials from Multiscale Perspective. *Adv. Energy Mater.* **2021**, *11*, 2003227. [CrossRef]
11. Manthiram, A. A Reflection on Lithium-Ion Battery Cathode Chemistry. *Nat. Commun.* **2020**, *11*, 1550. [CrossRef] [PubMed]

12. Wang, X.X.; Ding, Y.L.; Deng, Y.P.; Chen, Z.W. Ni-Rich/Co-Poor Layered Cathode for Automotive Li-Ion Batteries: Promises and Challenges. *Adv. Energy Mater.* **2020**, *10*, 1903864. [CrossRef]
13. Lu, Z.; Dahn, J.R. Understanding the Anomalous Capacity of $Li/LiNi_xLi_{(1/3-2x/3)}Mn_{(2/3-x/3)}O_2$ Cells Using In Situ X-ray Diffraction and Electrochemical Studies. *J. Electrochem. Soc.* **2002**, *149*, A815. [CrossRef]
14. Thackeray, M.M.; Kang, S.-H.; Johnson, C.S.; Vaughey, J.T.; Benedek, R.; Hackney, S.A. Li_2MnO_3-Stabilized $LiMO_2$ (M = Mn, Ni, Co) Electrodes for Lithium-Ion Batteries. *J. Mater. Chem.* **2007**, *17*, 3112–3125. [CrossRef]
15. Zheng, J.; Myeong, S.; Cho, W.; Yan, P.; Xiao, J.; Wang, C.; Cho, J.; Zhang, J.G. Li- and Mn-Rich Cathode Materials: Challenges to Commercialization. *Adv. Energy Mater.* **2016**, *7*, 1601284. [CrossRef]
16. Assat, G.; Tarascon, J.-M. Fundamental Understanding and Practical Challenges of Anionic Redox Activity in Li-Ion Batteries. *Nat. Energy* **2018**, *3*, 373–386. [CrossRef]
17. He, W.; Guo, W.B.; Wu, H.L.; Lin, L.; Liu, Q.; Han, X.; Xie, Q.S.; Liu, P.F.; Zheng, H.F.; Wang, L.S.; et al. Challenges and Recent Advances in High Capacity Li-Rich Cathode Materials for High Energy Density Lithium-Ion Batteries. *Adv. Mater.* **2021**, *33*, 2005937. [CrossRef]
18. Sathiya, M.; Rousse, G.; Ramesha, K.; Laisa, C.P.; Vezin, H.; Sougrati, M.T.; Doublet, M.L.; Foix, D.; Gonbeau, D.; Walker, W.; et al. Reversible Anionic Redox Chemistry in High-Capacity Layered-Oxide Electrodes. *Nat. Mater.* **2013**, *12*, 827–835. [CrossRef]
19. Luo, K.; Roberts, M.R.; Hao, R.; Guerrini, N.; Pickup, D.M.; Liu, Y.S.; Edstrom, K.; Guo, J.H.; Chadwick, A.V.; Duda, L.C.; et al. Charge-Compensation in 3d-Transition-Metal-Oxide Intercalation Cathodes through the Generation of Localized Electron Holes on Oxygen. *Nat. Chem.* **2016**, *8*, 684–691. [CrossRef]
20. Yu, X.; Lyu, Y.; Gu, L.; Wu, H.; Bak, S.-M.; Zhou, Y.; Amine, K.; Ehrlich, S.N.; Li, H.; Nam, K.-W.; et al. Understanding the Rate Capability of High-Energy-Density Li-Rich Layered $Li_{1.2}Ni_{0.15}Co_{0.1}Mn_{0.55}O_2$ Cathode Materials. *Adv. Energy Mater.* **2014**, *4*, 1300950. [CrossRef]
21. Assat, G.; Foix, D.; Delacourt, C.; Iadecola, A.; Dedryvere, R.; Tarascon, J.M. Fundamental Interplay between Anionic/Cationic Redox Governing the Kinetics and Thermodynamics of Lithium-Rich Cathodes. *Nat. Commun.* **2017**, *8*, 2219. [CrossRef] [PubMed]
22. Assat, G.; Iadecola, A.; Delacourt, C.; Dedryvère, R.; Tarascon, J.-M. Decoupling Cationic–Anionic Redox Processes in a Model Li-Rich Cathode Via Operando X-ray Absorption Spectroscopy. *Chem. Mater.* **2017**, *29*, 9714–9724. [CrossRef]
23. Hu, E.; Yu, X.; Lin, R.; Bi, X.; Lu, J.; Bak, S.; Nam, K.-W.; Xin, H.L.; Jaye, C.; Fischer, D.A.; et al. Evolution of Redox Couples in Li- and Mn-Rich Cathode Materials and Mitigation of Voltage Fade by Reducing Oxygen Release. *Nat. Energy* **2018**, *3*, 690–698. [CrossRef]
24. House, R.A.; Rees, G.J.; Pérez-Osorio, M.A.; Marie, J.-J.; Boivin, E.; Robertson, A.W.; Nag, A.; Garcia-Fernandez, M.; Zhou, K.-J.; Bruce, P.G. First-Cycle Voltage Hysteresis in Li-Rich 3d Cathodes Associated with Molecular O_2 Trapped in the Bulk. *Nat. Energy* **2020**, *5*, 777–785. [CrossRef]
25. Yang, J.; Muhammad, S.; Jo, M.R.; Kim, H.; Song, K.; Agyeman, D.A.; Kim, Y.-I.; Yoon, W.-S.; Kang, Y.-M. In Situ Analyses for Ion Storage Materials. *Chem. Soc. Rev.* **2016**, *45*, 5717–5770. [CrossRef]
26. Lin, F.; Liu, Y.; Yu, X.; Cheng, L.; Singer, A.; Shpyrko, O.G.; Xin, H.L.; Tamura, N.; Tian, C.; Weng, T.-C.; et al. Synchrotron X-ray Analytical Techniques for Studying Materials Electrochemistry in Rechargeable Batteries. *Chem. Rev.* **2017**, *117*, 13123–13186. [CrossRef]
27. Liu, D.; Shadike, Z.; Lin, R.; Qian, K.; Li, H.; Li, K.; Wang, S.; Yu, Q.; Liu, M.; Ganapathy, S.; et al. Review of Recent Development of In Situ/Operando Characterization Techniques for Lithium Battery Research. *Adv. Mater.* **2019**, *31*, e1806620. [CrossRef]
28. Ito, A.; Sato, Y.; Sanada, T.; Hatano, M.; Horie, H.; Ohsawa, Y. In Situ X-ray Absorption Spectroscopic Study of Li-Rich Layered Cathode Material $Li[Ni_{0.17}Li_{0.2}Co_{0.07}Mn_{0.56}]O_2$. *J. Power Sources* **2011**, *196*, 6828–6834. [CrossRef]
29. Yang, W.; Devereaux, T.P. Anionic and Cationic Redox and Interfaces in Batteries: Advances from Soft X-ray Absorption Spectroscopy to Resonant Inelastic Scattering. *J. Power Sources* **2018**, *389*, 188–197. [CrossRef]
30. Whittingham, M.S. Electrical Energy Storage and Intercalation Chemistry. *Science* **1976**, *192*, 1126–1127. [CrossRef]
31. Thackeray, M.M.; Johnson, P.J.; de Picciotto, L.A.; Bruce, P.G.; Goodenough, J.B. Electrochemical Extraction of Lithium from $LiMn_2O_4$. *Mater. Res. Bull.* **1984**, *19*, 179–187. [CrossRef]
32. Padhi, A.K.; Nanjundaswamy, K.S.; Goodenough, J.B. Phospho-Olivines as Positive-Electrode Materials for Rechargeable Lithium Batteries. *J. Electrochem. Soc.* **1997**, *144*, 1188–1194. [CrossRef]
33. Mizushima, K.; Jones, P.C.; Wiseman, P.J.; Goodenough, J.B. Li_xCoO_2 (0 <X <-1): A New Cathode Material for Batteries of High Energy Density. *Mater. Res. Bull.* **1980**, *15*, 783–789.
34. Dahn, J.R.; von Sacken, U.; Juzkow, M.W.; Al-Janaby, H. Rechargeable $LiNiO_2$/Carbon Cells. *J. Electrochem. Soc.* **1991**, *138*, 2207–2211. [CrossRef]
35. Lu, Z.; MacNeil, D.D.; Dahn, J.R. Layered $LiNi_xCo_{1-2x}Mn_xO_2$ Cathode Materials for Lithium-Ion Batteries. *Electrochem. Solid-State Lett.* **2001**, *4*, A200–A203. [CrossRef]
36. Ohzuku, T.; Makimura, Y. Layered Lithium Insertion Material of $LiCo_{1/3}Ni_{1/3}Mn_{1/3}O_2$ for Lithium-Ion Batteries. *Chem. Lett.* **2001**, *30*, 642–643. [CrossRef]
37. Bak, S.-M.; Shadike, Z.; Lin, R.; Yu, X.; Yang, X.-Q. In Situ/Operando Synchrotron-Based X-ray Techniques for Lithium-Ion Battery Research. *NPG Asia Mater.* **2018**, *10*, 563–580. [CrossRef]
38. Fadley, C.S. X-ray Photoelectron Spectroscopy: Progress and Perspectives. *J. Electron Spectrosc. Relat. Phenom.* **2010**, *178–179*, 2–32. [CrossRef]

39. Stevie, F.A.; Donley, C.L. Introduction to X-ray Photoelectron Spectroscopy. *J. Vac. Sci. Technol. A* **2020**, *38*, 063204. [CrossRef]
40. Assat, G.; Iadecola, A.; Foix, D.; Dedryvère, R.; Tarascon, J.-M. Direct Quantification of Anionic Redox over Long Cycling of Li-Rich NMC Via Hard X-ray Photoemission Spectroscopy. *ACS Energy Lett.* **2018**, *3*, 2721–2728. [CrossRef]
41. Naylor, A.J.; Makkos, E.; Maibach, J.; Guerrini, N.; Sobkowiak, A.; Björklund, E.; Lozano, J.G.; Menon, A.S.; Younesi, R.; Roberts, M.R.; et al. Depth-Dependent Oxygen Redox Activity in Lithium-Rich Layered Oxide Cathodes. *J. Mater. Chem. A* **2019**, *7*, 25355–25368. [CrossRef]
42. Rehr, J.J.; Albers, R.C. Theoretical Approaches to X-ray Absorption Fine Structure. *Rev. Mod. Phys.* **2000**, *72*, 621–654. [CrossRef]
43. Dau, H.; Liebisch, P.; Haumann, M. X-ray Absorption Spectroscopy to Analyze Nuclear Geometry and Electronic Structure of Biological Metal Centers—Potential and Questions Examined with Special Focus on the Tetra-Nuclear Manganese Complex of Oxygenic Photosynthesis. *Anal. Bioanal. Chem.* **2003**, *376*, 562–583. [CrossRef] [PubMed]
44. Farges, F. Ab Initio and Experimental Pre-Edge Investigations of the Mn K-Edge Xanes in Oxide-Type Materials. *Phys. Rev. B* **2005**, *71*, 155109. [CrossRef]
45. Koga, H.; Croguennec, L.; Menetrier, M.; Mannessiez, P.; Weill, F.; Delmas, C.; Belin, S. Operando X-ray Absorption Study of the Redox Processes Involved Upon Cycling of the Li-Rich Layered Oxide $Li_{1.20}Mn_{0.54}Co_{0.13}Ni_{0.13}O_2$ in Li Ion Batteries. *J. Phys. Chem. C* **2014**, *118*, 5700–5709. [CrossRef]
46. Luo, K.; Roberts, M.R.; Guerrini, N.; Tapia-Ruiz, N.; Hao, R.; Massel, F.; Pickup, D.M.; Ramos, S.; Liu, Y.S.; Guo, J.; et al. Anion Redox Chemistry in the Cobalt Free 3d Transition Metal Oxide Intercalation Electrode $Li[Li_{0.2}Ni_{0.2}Mn_{0.6}]O_2$. *J. Am. Chem. Soc.* **2016**, *138*, 11211–11218. [CrossRef]
47. Nam, K.-W.; Kim, M.G.; Kim, K.-B. In Situ Mn K-Edge X-ray Absorption Spectroscopy Studies of Electrodeposited Manganese Oxide Films for Electrochemical Capacitors. *J. Phys. Chem. C* **2007**, *111*, 749–758. [CrossRef]
48. Gilbert, B.; Frazer, B.H.; Belz, A.; Conrad, P.G.; Nealson, K.H.; Haskel, D.; Lang, J.C.; Srajer, G.; De Stasio, G. Multiple Scattering Calculations of Bonding and X-ray Absorption Spectroscopy of Manganese Oxides. *J. Phys. Chem. A* **2003**, *107*, 2839–2847. [CrossRef]
49. Hy, S.; Su, W.-N.; Chen, J.-M.; Hwang, B.-J. Soft X-ray Absorption Spectroscopic and Raman Studies on $Li_{1.2}Ni_{0.2}Mn_{0.6}O_2$ for Lithium-Ion Batteries. *J. Phys. Chem. C* **2012**, *116*, 25242–25247. [CrossRef]
50. Ohmer, N.; Fenk, B.; Samuelis, D.; Chen, C.-C.; Maier, J.; Weigand, M.; Goering, E.; Schütz, G. Phase Evolution in Single-Crystalline $LiFePO_4$ Followed by in Situ Scanning X-ray Microscopy of a Micrometre-Sized Battery. *Nat. Commun.* **2015**, *6*, 6045. [CrossRef]
51. Gent, W.E.; Lim, K.; Liang, Y.; Li, Q.; Barnes, T.; Ahn, S.J.; Stone, K.H.; McIntire, M.; Hong, J.; Song, J.H.; et al. Coupling between Oxygen Redox and Cation Migration Explains Unusual Electrochemistry in Lithium-Rich Layered Oxides. *Nat. Commun.* **2017**, *8*, 2091. [CrossRef] [PubMed]
52. Maitra, U.; House, R.A.; Somerville, J.W.; Tapia-Ruiz, N.; Lozano, J.G.; Guerrini, N.; Hao, R.; Luo, K.; Jin, L.; Perez-Osorio, M.A.; et al. Oxygen Redox Chemistry without Excess Alkali-Metal Ions in $Na_{2/3}[Mg_{0.28}Mn_{0.72}]O_2$. *Nat. Chem.* **2018**, *10*, 288–295. [CrossRef] [PubMed]
53. Zuba, M.J.; Grenier, A.; Lebens-Higgins, Z.; Fajardo, G.J.P.; Li, Y.; Ha, Y.; Zhou, H.; Whittingham, M.S.; Yang, W.; Meng, Y.S.; et al. Whither Mn Oxidation in Mn-Rich Alkali-Excess Cathodes? *ACS Energy Lett.* **2021**, *6*, 1055–1064. [CrossRef]
54. Fang, L.; Zhou, L.; Park, M.; Han, D.; Lee, G.-H.; Kang, S.; Lee, S.; Chen, M.; Hu, Z.; Zhang, K.; et al. Hysteresis Induced by Incomplete Cationic Redox in Li-Rich 3d-Transition-Metal Layered Oxides Cathodes. *Adv. Sci.* **2022**, *9*, 2201896. [CrossRef] [PubMed]
55. Hong, J.; Gent, W.E.; Xiao, P.; Lim, K.; Seo, D.H.; Wu, J.; Csernica, P.M.; Takacs, C.J.; Nordlund, D.; Sun, C.J.; et al. Metal-Oxygen Decoordination Stabilizes Anion Redox in Li-Rich Oxides. *Nat. Mater.* **2019**, *18*, 256–265. [CrossRef]
56. Lebens-Higgins, Z.W.; Vinckeviciute, J.; Wu, J.; Faenza, N.V.; Li, Y.; Sallis, S.; Pereira, N.; Meng, Y.S.; Amatucci, G.G.; Der Ven, A.V.; et al. Distinction between Intrinsic and X-ray-Induced Oxidized Oxygen States in Li-Rich 3d Layered Oxides and $LiAlO_2$. *J. Phys. Chem. C* **2019**, *123*, 13201–13207. [CrossRef]
57. Zhang, J.-N.; Li, Q.; Ouyang, C.; Yu, X.; Ge, M.; Huang, X.; Hu, E.; Ma, C.; Li, S.; Xiao, R.; et al. Trace Doping of Multiple Elements Enables Stable Battery Cycling of $LiCoO_2$ at 4.6 V. *Nat. Energy* **2019**, *4*, 594–603. [CrossRef]
58. Eum, D.; Kim, B.; Kim, S.J.; Park, H.; Wu, J.; Cho, S.P.; Yoon, G.; Lee, M.H.; Jung, S.K.; Yang, W.; et al. Voltage Decay and Redox Asymmetry Mitigation by Reversible Cation Migration in Lithium-Rich Layered Oxide Electrodes. *Natrue Mater.* **2020**, *19*, 419–427. [CrossRef]
59. House, R.A.; Maitra, U.; Pérez-Osorio, M.A.; Lozano, J.G.; Jin, L.; Somerville, J.W.; Duda, L.C.; Nag, A.; Walters, A.; Zhou, K.-J.; et al. Superstructure Control of First-Cycle Voltage Hysteresis in Oxygen-Redox Cathodes. *Nature* **2020**, *577*, 502–508. [CrossRef]
60. Lee, G.-H.; Wu, J.; Kim, D.; Cho, K.; Cho, M.; Yang, W.; Kang, Y.-M. Reversible Anionic Redox Activities in Conventional $LiNi_{1/3}Co_{1/3}Mn_{1/3}O_2$ Cathodes. *Angew. Chem. Int. Ed. Engl.* **2020**, *59*, 8681–8688. [CrossRef]
61. Rana, J.; Papp, J.K.; Lebens-Higgins, Z.; Zuba, M.; Kaufman, L.A.; Goel, A.; Schmuch, R.; Winter, M.; Whittingham, M.S.; Yang, W.; et al. Quantifying the Capacity Contributions During Activation of Li_2MnO_3. *ACS Energy Lett.* **2020**, *5*, 634–641. [CrossRef]
62. House, R.A.; Marie, J.-J.; Park, J.; Rees, G.J.; Agrestini, S.; Nag, A.; Garcia-Fernandez, M.; Zhou, K.-J.; Bruce, P.G. Covalency Does Not Suppress O_2 Formation in 4d and 5d Li-Rich O-Redox Cathodes. *Nat. Commun.* **2021**, *12*, 2975. [CrossRef] [PubMed]
63. Wang, Q.; Mariyappan, S.; Rousse, G.; Morozov, A.V.; Porcheron, B.; Dedryvère, R.; Wu, J.; Yang, W.; Zhang, L.; Chakir, M.; et al. Unlocking Anionic Redox Activity in O_3-Type Sodium 3d Layered Oxides Via Li Substitution. *Nat. Mater.* **2021**, *20*, 353–361. [CrossRef] [PubMed]

64. Rossouw, M.H.; Thackeray, M.M. Lithium Manganese Oxides from Li_2MnO_3 for Rechargeable Lithium Battery Applications. *Mater. Res. Bull.* **1991**, *26*, 463–473. [CrossRef]
65. Rana, J.; Stan, M.; Kloepsch, R.; Li, J.; Schumacher, G.; Welter, E.; Zizak, I.; Banhart, J.; Winter, M. Structural Changes in Li_2MnO_3 Cathode Material for Li-Ion Batteries. *Adv. Energy Mater.* **2014**, *4*, 1300998. [CrossRef]
66. Foix, D.; Sathiya, M.; McCalla, E.; Tarascon, J.-M.; Gonbeau, D. X-ray Photoemission Spectroscopy Study of Cationic and Anionic Redox Processes in High-Capacity Li-Ion Battery Layered-Oxide Electrodes. *J. Phys. Chem. C* **2016**, *120*, 862–874. [CrossRef]
67. Li, B.; Shao, R.; Yan, H.; An, L.; Zhang, B.; Wei, H.; Ma, J.; Xia, D.; Han, X. Understanding the Stability for Li-Rich Layered Oxide Li_2RuO_3 Cathode. *Adv. Funct. Mater.* **2016**, *26*, 1330–1337. [CrossRef]
68. Kobayashi, H.; Kanno, R.; Tabuchi, M.; Kageyama, H.; Nakamura, O.; Takano, M. Structure and Charge/Discharge Characteristics of New Layered Oxides: $Li_{1.8}Ru_{0.6}Fe_{0.6}O_3$ and Li_2IrO_3. *J. Power Sources* **1997**, *68*, 686–691. [CrossRef]
69. McCalla, E.; Abakumov Artem, M.; Saubanère, M.; Foix, D.; Berg Erik, J.; Rousse, G.; Doublet, M.-L.; Gonbeau, D.; Novák, P.; Van Tendeloo, G.; et al. Visualization of O-O Peroxo-Like Dimers in High-Capacity Layered Oxides for Li-Ion Batteries. *Science* **2015**, *350*, 1516–1521. [CrossRef]